Experimental investigations on macrocell corrosion in chloride-contaminated concrete

J.J.W. Gulikers
Delft University of Technology, Faculty of Civil Engineering, Stevin Laboratory

Chloride-induced reinforcement corrosion in concrete is characterised by the action of so-called macrocells. The associated localised form of corrosion results from the strong electrochemical interaction between the relatively small pitting sites acting as anodes and the large passive steel areas acting as cathodes. The existence of macrocell corrosion poses severe problems in the interpretation of results obtained from corrosion experiments, especially regarding corrosion potential and galvanic current.
To elucidate the mechanism of macrocell corrosion experimental investigations were conducted on reinforcement steel embedded in chloride-contaminated concrete. The macrocells were provoked by shortcircuiting actively corroding mild steel bars to passivated stainless steel, thereby intensifying the corrosion process. The experiments included measurement of corrosion potential, ionic concrete resistance, potential difference, corrosion rate and galvanic current.
The magnitude of the galvanic current is significantly influenced by the resistance of passive steel to polarisation, and to a much lesser degree by the ionic concrete resistance. Results from potential mapping demonstrated that due to macrocell action the rest potential of the passive steel was shifted towards very negative values that, according to many codes of practice, would suggest active corrosion to take place.

Keywords: **concrete, reinforcing steel, chloride, durability, corrosion, macrocell testing**

Introduction

Under the normal conditions prevailing in concrete the embedded reinforcing steel is effectively prevented from corrosion by the highly alkaline nature of the concrete pore water solution and the presence of dissolved oxygen. In this environment a stable and tightly adhering iron oxide film is formed on the surface which renders the steel essentially passive. In addition, concrete can be proportioned to have a low permeability which minimizes the penetration of corrosion-inducing substances from the ambient environment. Because of these inherent protective attributes, corrosion of embedded steel does not occur in the vast majority of reinforced concrete elements or structures during their service life.
Although most concrete structures perform satisfactorily for over 50 years, there is now a world-wide problem of deterioration caused primarily by corrosion of the embedded reinforcement steel. The deterioration due to corrosion results because the corrosion products (rust) occupy a much

larger volume than the steel consumed. Delamination and spalling of the concrete cover occur due to its inability to accommodate the generated tensile stresses. With time, structural distress may occur either by loss of bond between the steel and concrete due to cracking and spalling, or as a result of reduced steel cross-sectional area. The main causes of this international, costly problem are identified as a lack of understanding of the corrosion mechanisms by the engineer and poor support from research establishments to assess the problem and produce solutions, see Browne (1991).

One of the more common modes of deterioration associated with reinforced concrete is due to chloride-induced corrosion of the embedded reinforcing steel. Chlorides may be introduced into concrete through accelerating admixtures, chloride-contaminated aggregates or brackish mixing water. Chlorides may also enter into concrete subsequently, by de-icing salts in bridge decks and parking structures, from sea water in marine structures, or from saline soil and ground water. To initiate corrosion, free chlorides must be present in sufficient concentration in the vicinity of the steel-concrete interface. The chloride ions can cause the local breakdown of the passive film at the steel-concrete interface resulting in aggressive corrosion over a limited area. The ensuing localised form of corrosion is known as pitting and is characterised by galvanic (macrocell) action between relative large areas of passive steel acting as cathode and small anodic pits. Within the pits, a local environment develops with a high chloride concentration, a depressed oxygen availability and a low pH value. Due to the large area ratios between anodic and adjoining cathodic areas high rates of attack occur within the pit.
Given the large dimensions of real structures most practical problems of reinforcement corrosion usually involve some kind of macrocell action in which anodic and cathodic regions on the steel surface are spatially separated, see Andrade et al. (1992). The existence of macrocells is a phenomenon usually not encountered in the small test-sized specimens that are normally studied in the laboratory. Despite the practical significance of macrocell corrosion to reinforced concrete deterioration, relatively little effort has been directed towards investigating this type of corrosion. In the following experimental investigations are described aimed at elucidating and quantifying macrocell corrosion in chloride-contaminated concrete.

Electrochemical theory of macrocell corrosion in concrete

The corrosion of steel in concrete is essentially electrochemical in nature, i.e., the corrosion process ordinarily proceeds by forming electrochemical cells with anodic and cathodic areas on the steel surface. The anodic (oxidation) and cathodic (reduction) reactions occur simultaneously in which electrical charge is transferred through the steel-concrete interface with an overall electrical charge balance being maintained within the system. In this respect the surface of the corroding reinforcement functions as a mixed electrode being a composite of anodic and cathodic sites electrically interconnected through the body of the steel itself (electron conduction) and the concrete pore solution (ion conduction).

For corrosion of steel reinforcement the anodic process is related to the dissolution of iron, passing into the concrete pore solution as positively charged divalent ferrous ions and leaving free electrons in the metal, according to the oxidation reaction:

$$Fe \rightarrow Fe^{+2} + 2e^{-} \tag{1}$$

The excess free electrons flow through the body of the steel reinforcement to the cathodic sites where they are consumed in a reduction reaction. In the highly alkaline environment normally present in concrete, it is commonly accepted that the prevailing cathodic reaction is the reduction of oxygen, according to:

$$O_2 + 2H_2O + 4e^{-} \rightarrow 4OH^{-} \tag{2}$$

Concrete structures freely exposed to the atmosphere usually have an adequate supply of oxygen diffusing through the concrete cover to support the cathodic reactions. The hydroxyl-ions produced in the cathodic reactions migrate under the influence of an electrical field towards the anodic sites where they neutralise the dissolved ferrous ions to form a fairly soluble ferrous hydroxide. Given sufficient oxygen, this product can be further oxidised to voluminous forms of insoluble hydrated rust. The corrosion process in reinforced concrete is illustrated in Fig. 1.

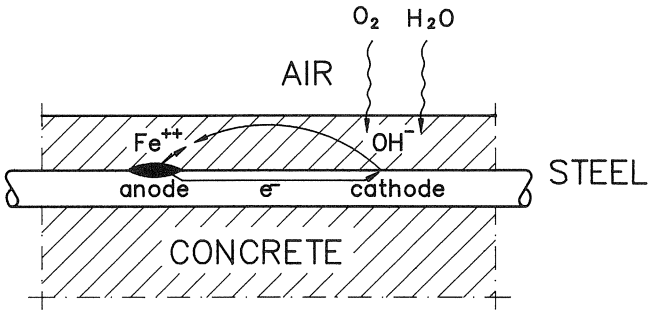

Fig. 1. Corrosion process of steel reinforcement in concrete.

The anode reactions must generate electrons at exactly the same rate as they are consumed in the cathodic reactions, so that in practice the rate at which the iron is dissolved can be controlled by the kinetics (speed) of either the anodic or cathodic reactions. The corrosion rate can be related to the rate at which negatively charged electrons are produced, i.e. the anodic or corrosion current density, i_a [μA/cm^2]. The rate of attack can be calculated from the corrosion current density using Faraday's Law; a current density of 1 A/m^2 corresponds to a loss of about 1 mm/year. According to Alonso et al. (1988), corrosion current densities exceeding 0.1–0.2 μA/cm^2 are considered to correspond with significant corrosion rates.

As corrosion is an electrochemical process, for the reactions to occur it is also essential that within the steel-concrete system differences exist in electrochemical potential between adjacent steel areas. These differences in potential can arise from inherent differences in the concrete and steel itself or from differences in the exposure conditions of the concrete. In general, electrochemical cells develop due to variations in salt concentration in the pore water or due to a non-uniform access of oxygen. In this respect a differentiation can be made between micro- and macro-corrosion cells. The former are characterised by the microscopic distance between local anodes and cathodes. Moreover, the minuscule anodic and cathodic sites cannot be distinguished and are randomly distributed over the complete surface area of the corroding bar. Since the anodic and cathodic reactions proceed on the steel surface directly side by side, micro-corrosion cells normally give rise to a uniform corrosion rate. For carbonation-induced corrosion it is likely that micro-corrosion cells will develop. For such a cell, only the mixed potentials of the numerous anodes and cathodes can be measured.
Local differences in concrete cover, environmental conditions, concrete permeability and other factors combine to cause a potential difference between larger steel areas, which in turn may lead to the formation of macro-corrosion cells. Practical examples of reinforcement corrosion include differential aeration and active/passive cells, see Gulikers et al. (1992).
A macrocell is defined by the size of the anodic and cathodic regions, which is of the same order of the surface area of the corroding bar, as is the distance between macro-anodes and macro-cathodes, see González et al. (1988). In a macrocell both the anodic and cathodic potentials can be measured, and the galvanic current I_{gal} flowing through the steel from the cathodic to the anodic region gives the required overall electrical charge balance. Only when the cathodic processes can be eliminated completely on the anodic component the magnitude of the galvanic current is a direct measure of the corrosion rate of the anodic component.
In laboratory experiments, these kind of macrocells are frequently used to investigate the development of the corrosion rate over time, see Schießl et al. (1990), and Raupach (1992). However, a direct conversion can be made only for ideal situations which rarely occur under practical conditions. This is due to the fact that both the anodic and cathodic component making up a galvanic cell still have to be considered as a mixed electrode whereupon anodic as well as cathodic reactions occur. Consequently, for real structures the measured galvanic current can severely underestimate the true corrosion activity of the anodic component.

Analytical description of macrocell corrosion

Macrocell corrosion results from potential differences that exist between steel sections being in electrical (steel) and electrolytical (concrete) contact. The more base region of the reinforcement develops as the anodic component whereas the more noble steel region turns into the cathodic component. For a cathodic component of a macrocell the reduction reactions predominate as to give a net consumption of electrons, whereas for an anodic component the iron dissolution reactions prevail which results in a net production of electrons.
In a simplified way the magnitude of the galvanic current I_{gal}, flowing in a two component macrocell, can be expressed (mathematically) by:

$$I_{gal} = \frac{E^c_{corr} - E^a_{corr}}{R^a_p + R_{con} + R^p_c} = \frac{U_{oc}}{R_{cell}} \qquad (3)$$

The driving macrocell voltage, $U_{oc} = (E^c_{corr} - E^a_{corr})$, is measured as the potential difference between the cathodic and anodic component prior to coupling. The magnitude of I_{gal} is not only dependent on the cell voltage U_{oc}, but also on electrochemical (kinetic hindrance) and geometrical (cathodic to anodic surface area ratio) parameters. The resistances associated with the cathodic, electrolytic, and anodic retardations are represented by R^c_p, R_{con}, and R^a_p, respectively.
The electrochemical interaction between steel regions with different steady-state potentials can be explained graphically by superimposing the potential-current (*E–I*) or polarisation curves for the anodic and cathodic component in a so-called Evans-diagram (see Fig. 2). As a consequence of macrocell action the potential of the anodic component is shifted towards less negative values (anodic polarisation) and the potential of the cathodic component is shifted towards less positive values (cathodic polarisation). From the points of intersection of the polarisation curves, the potentials of the coupled steel electrodes and the galvanic current can be derived.

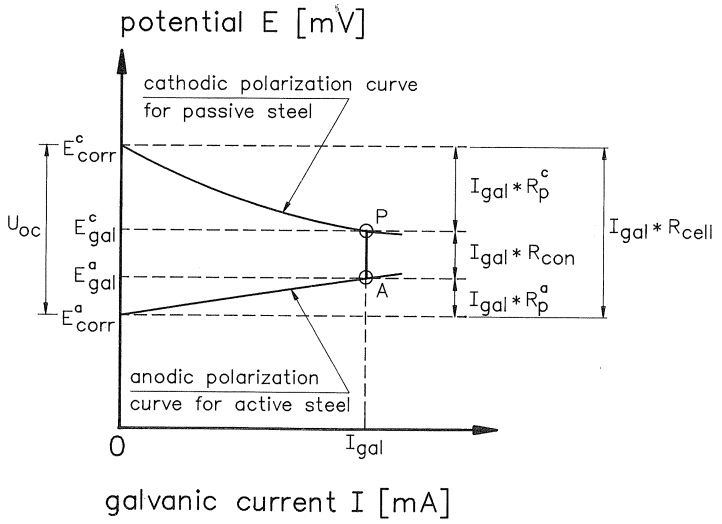

Fig. 2. Evans-diagram for a two-component macrocell.

For active/passive corrosion cells the resistance to cathodic polarisation of passive steel, R^c_p, is likely to be several orders of magnitude larger than the polarisation resistance of corroding steel. In general, the electrochemical resistances of steel electrodes are dependent on the magnitude of the galvanic current. Given a certain geometrical electrode configuration the value of the concrete resistance, R_{con}, can be considered to be independent on the magnitude of I_{gal}. An evaluation of the

influence of the individual resistances on macrocell action is only possible when, besides the magnitude of I_{gal}, also reliable values for U_{oc} and R_{con} are available.

At the steady-state or open-circuit potential E_{corr} of a reinforcement steel section there is no external electric interference and consequently no net transfer of electric charge. Thus, the average anodic and cathodic current density (i_a and i_c respectively) balance and are equal to the corrosion current density i_{corr}. However, if the steel section is displaced from its steady-state potential by macrocell action, the resulting polarisation stimulates the oxidation or reduction reactions at the steel surface. In general, if the potential E becomes more positive than its initial steady-state potential E_{corr} (anodic polarisation), then the anodic iron dissolution reaction is encouraged and simultaneously the cathodic reactions are hindered. The relationship between polarising external current I_{app} and the potential E of a steel section can be described in a simplified way by:

$$I_{app} = A_{exp}[i_a + i_c]$$

$$= A_{exp} i_{corr}\left[\exp\left(\frac{\ln(10)(E - E_{corr})}{b_a}\right) - \exp\left(\frac{-\ln(10)(E - E_{corr})}{b_c}\right)\right] \quad (4)$$

where b_a and b_c are the so-called Tafel slopes for the anodic and cathodic reactions occurring at the steel surface, and A_{exp} the exposed surface area of the steel electrode. Based on empirically derived values, see Andrade et al. (1986), it can be assumed that for corroding steel $b_a = 90$ mV / dec and $b_c = 180$ mV / dec.

Equation (3) provides the basis for the so-called linear polarisation technique normally used for estimating the instantaneous corrosion rate. Polarisation characteristics can be measured by plotting the external current as a function of the electrochemical potential.

The actual corrosion rate is always equal to the anodic current density i_a which is related to the overvoltage ($E - E_{corr}$) achieved, according to:

$$i_a = i_{corr} \cdot \exp\left(\frac{\ln(10)(E - E_{corr})}{b_a}\right) \quad (5)$$

in which i_{corr} refers to the initial corrosion current density, i.e. without any external polarisation. The corrosion rate is increased when anodic polarisation occurs and decreased for cathodic polarisation. The relationships between galvanic current I_{gal}, actual corrosion rate I_a, and initial corrosion rate I_{corr}, are given in Fig. 3. In general, the actual corrosion rate is underestimated by the galvanic current, the difference becoming larger as the anodic overvoltage decreases. For anodic overvoltages exceeding 50 mV, the magnitude of the galvanic current may be considered to be nearly equal to the actual corrosion rate I_a.

The operation of a macrocell essentially results in a shift from the original steady-state potentials of the participating components. If the magnitude of the overvoltage is known it will be possible to relate the galvanic current into the initial corrosion rates, based on the given electrochemical relationships, see Gulikers et al. (1994).

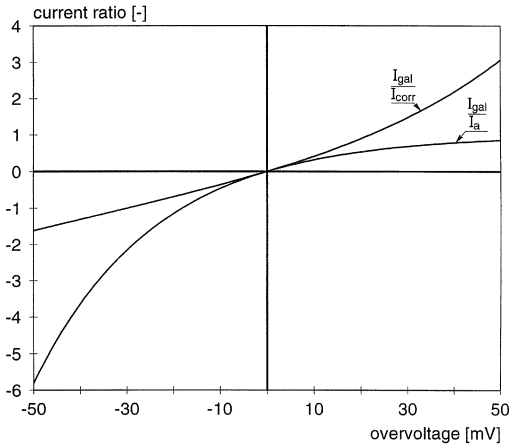

Fig. 3. Current – overvoltage relationships for corroding steel.

Design of the concrete corrosion cell

In order to investigate the susceptibility to galvanic reinforcement corrosion in chloride-contaminated concrete, specimens were developed which incorporated actively corroding and passive steel reinforcement bars. The basic design criterion was that in the cell the real case of corroding (anodic) steel areas, and its associated passive (cathodic) steel regions of a reinforcement network in concrete partially contaminated with an excess amount of chloride should be simulated. An isometric sketch of the experimental arrangement is illustrated in Fig. 4. In these specimens macrocell action is induced between the top and bottom layer of reinforcement. Chloride and moisture enter the concrete from the top surface and will promote active corrosion of the top layer. The bottom layer of reinforcement remains essentially passive, and, being surrounded by a drier environment with consequently more access to oxygen, will be cathodic to the top layer.

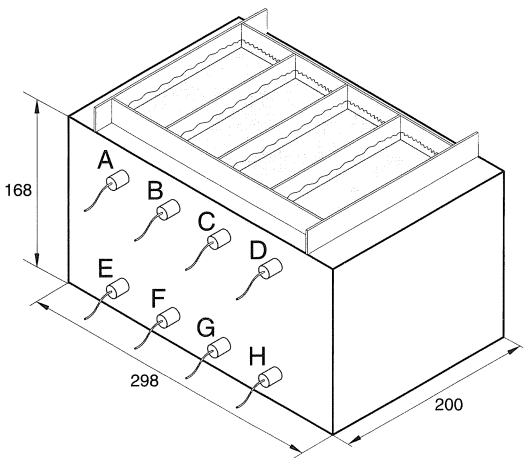

Fig. 4. Isometric sketch of a concrete corrosion cell.

The specimens were 298 mm (width) by 168 mm (height) by 200 mm (depth) in dimensions.
Two layers of reinforcing bars were incorporated in each specimen, both with 25 mm clear cover. The top layer contained four mild steel bars ø 6 mm with exposure lengths of 25, 50, 75 and 100 mm, respectively, placed at variable positions designated by A, B, C and D. The bottom layer consisted of four stainless steel bars ø 12 mm with a fixed exposure length of 100 mm, located at positions designated by E, F, G and H. The horizontal centre-to-centre distance between the steel bars was 62 mm and the vertical distance was 109 mm. Plexiglass dikes, 25 mm high, were mounted on the top surface of each specimen for ponding.
For convenience chloride was added to the mixing water in an excess amount of 4% Cl^- by weight of cement which rendered the complete concrete specimen corrosive to mild steel. For this reason AISI type 316 stainless steel was chosen for the bottom layer. This type of steel will remain essentially passive whatever the condition of the concrete and shows a similar electrochemical behaviour as a mild steel reinforcing bar in chloride-free concrete, see Naish et al. (1990).
Four batches, each consisting of four specimens, were fabricated with portland and blast furnace slag cement (slag content of 75%). All concrete was batched according to the mix design given in the Appendix. The specimens were cured for two days in the moulds followed by 12 days of air-drying at 50% R.H. and 20°C. Thereupon, the four vertical sides of each specimen were given two layers of a commercially available two-component epoxy concrete sealer to minimise humidity and oxygen exchange with the ambient environment. The treated specimens were initially exposed to constant relative humidities of approximately 98% R.H. and 80% R.H. at a constant ambient temperature of 20°C.
The potential difference between corroding mild steel and passive stainless steel will generate galvanic currents between the two zones which will normally result in an acceleration of the local corrosion rates of the top steel layer.

Experimental test methods

The corrosion cell was designed to monitor the factors that were expected to exert some influence on the galvanic corrosion process of steel in a concrete environment. Hence, provisions were made for measuring:
- E_{corr}, the electrochemical corrosion potential (i.e. against a reference electrode);
- U_{oc}, the driving macrocell voltage developed between corroding and passive steel bars;
- R_{con}, the concrete resistance between corroding and passive steel bars;

and
- I_{gal}, the galvanic (or macrocell) corrosion current.

One of the specimens fabricated with blast furnace slag cement was employed for detailed investigations on macrocell corrosion. Some of the results obtained from this galvanic testing will be reported here. The other test results will be published in the near future, see e.g. Gulikers (1997a) and Gulikers (1997b).
The actively corroding mild steel bars are referred to as ACT followed by the exposure length (25, 50, 75 and 100, respectively). The passive stainless steel bars (with a constant exposure length of

100 mm) are indicated by PAS followed by the exposure length of the mild steel bar located at the opposite side. The location of the individual rebars in the concrete specimen is given in Table 1.

Table 1. Location of steel bars in concrete specimen.

top ø6 mm	A ACT50	B ACT75	C ACT100	D ACT25
bottom	PAS50	PAS75	PAS100	PAS25
l_{exp} = 100 mm ø12 mm	E	F	G	H

The compartment at location B (above rebar ACT75) was previously ponded with tap water for more than 3 months.
The test procedure included measurement of E_{corr} and U_{oc} prior to performing galvanic coupling, whereas the concrete resistance was measured at the end of testing.

Experimental results

Determination of a modified Evans-diagram
The experimental investigations were aimed at a quantitative determination of the resistances involved in a macrocell, as defined by Eq. (3). One corroding and one passive steel bar were coupled through an external circuit as to form a two-component macrocell. Prior to coupling, the open-circuit potential difference U_{oc} was measured. In order to achieve a stepwise increase of the cell voltage U_{cell} a voltage source was inserted into the external circuit. When the cell voltage equals the open-circuit potential difference, the natural condition of shortcircuiting is achieved. With this instrumental test set-up it is possible to realize cell voltages far beyond U_{oc} in order to study the polarisation behaviour of both passive and corroding steel over a wide range of overvoltages.
For circuit ACT75-PAS75, U_{oc} amounted to 321.5 mV and R_{con} was 6444 Ω. Rebar ACT75 demonstrated a much lower corrosion potential, E_{corr} = –278 mV (vs. Ag/AgCl), compared to the other three corroding rebars.
The average cell resistance R_{cell} was calculated for each value of U_{cell} by:

$$R_{cell} = \frac{U_{cell}}{I_{cell}} \tag{6}$$

The cell current flowing through the artificially enforced macrocell was measured by a Zero-Resistance-Ammeter (ZRA). This measuring device allows continuous monitoring of a current without placing any resistive load on the electrochemical system (to avoid artificial polarisation of the anodic and cathodic components of the macrocell).

In Fig. 5 the resulting cell current I_{cell} is presented as a function of U_{cell}. The graph shows a very pronounced exponential increase of I_{cell} as U_{cell} is becoming larger. Beyond a cell voltage of approximately 300 mV the cell current increases significantly.

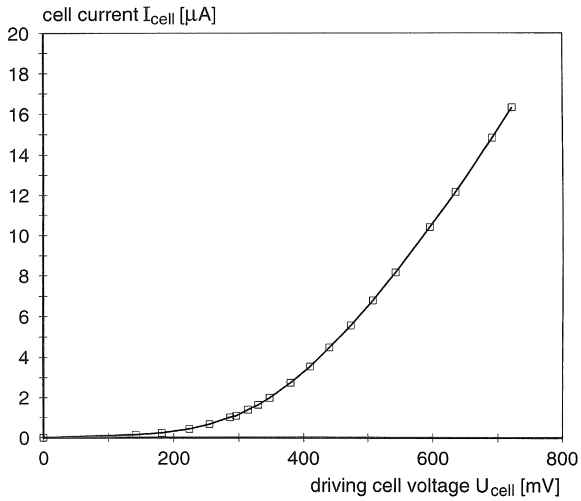

Fig. 5. Development of the cell current I_{cell} as a function of the imposed macrocell voltage U_{cell}.

In Fig. 6 the calculated cell resistance, R_{cell}, is displayed as a function of U_{cell}. Given the trend discussed before it is not surprising that an exponential decrease occurs. Initially, at low values for U_{cell}, the cell resistance is very high. For U_{cell} = 142 mV a cell resistance of R_{cell} = 930.7 kΩ was calculated, and at the highest value for U_{cell} = 722 mV, R_{cell} = 34.8 kΩ. These calculated values clearly indicate that within the full range of U_{cell} the cell resistance is much larger than R_{con} (6444 Ω). Taking into account the concrete resistance, the anodic and cathodic overvoltages of the corroding and passive steel, respectively, could be calculated. The polarisation resistance of the corroding rebar $R_{p,a}$ shows a gradual increase from 880 Ω to 2951 Ω as the overvoltage increases. The resistance against cathodic polarisation of the passive stainless steel bar contributes to a significant extent to the overall cell resistance. This trend is also observed for all other macrocell couples.
Since the concrete resistance remains essentially constant during the experiments and the polarisation resistance of the corroding mild steel is considered to be small compared to that of the passive steel bar, it is concluded that $R_{p,c}$ controls to a large extent the magnitude of the galvanic current flowing in a macrocell with a plan-parallel configuration of electrodes in most practical situations. This is also shown in Fig. 7 where the relative control exerted by the three resistances is given as a function of the cell voltage. For U_{cell} = 700 mV, which is far beyond practical values for U_{oc}, the control exercised by the passive steel bar still amounts to 80%, whereas the corroding steel bar contributes just 6%, and the concrete resistance 14% to R_{cell}.
From the relationships between overvoltage and current derived for both passive and corroding steel a modified Evans-diagram is constructed for the circuit ACT75-PAS75 (see Fig. 8). Arbitrarily,

the initial potential of passive steel is assigned 0. Without macrocell action the initial potential difference amounts to 321.5 mV. The galvanic current I_{gal} expected to flow in the circuit when the two bars are shortcircuited, can be calculated to be approximately 1.47 μA (taking into account the voltage drop over the concrete electrolyte). After the experiments were completed, shortcircuiting was effected. After a few hours steady- state conditions were achieved with I_{gal} = 1.36 μA which is close to the predicted value.

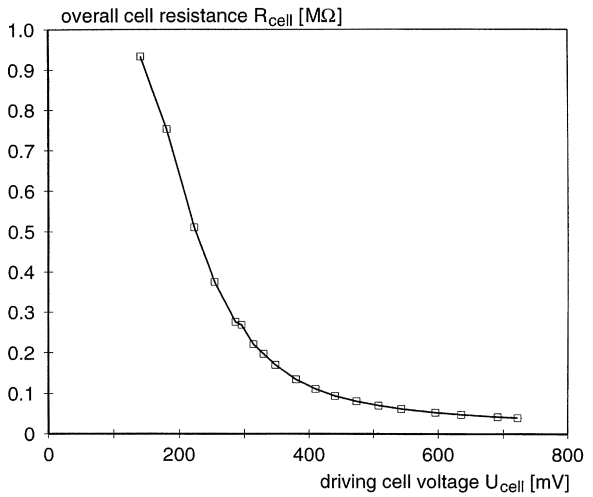

Fig. 6. Development of the overall cell resistance R_{cell} as a function of the imposed macrocell voltage U_{cell}.

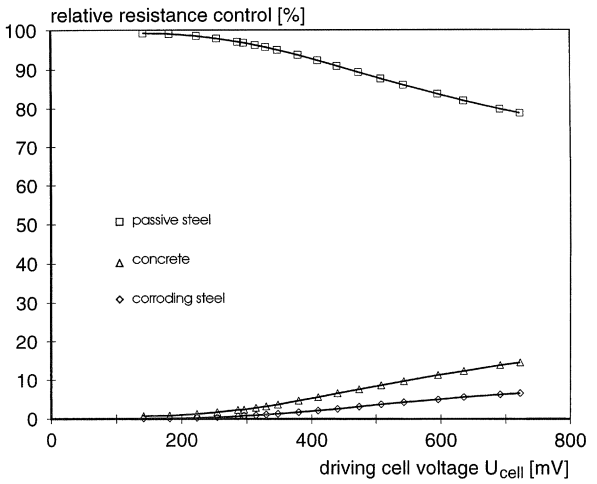

Fig. 7. Development of the relative influence of the individual resistances on the overall cell resistance R_{cell} as a function of the imposed macrocell voltage U_{cell}.

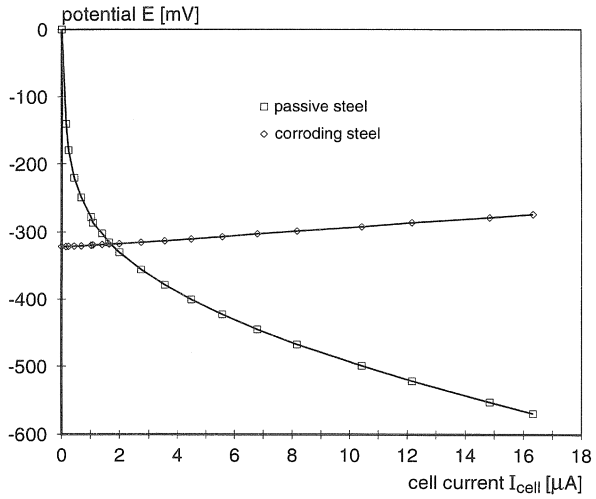

Fig. 8. Modified Evans-diagram for active/passive macrocell ACT75-PAS75.

Influence of macrocells on corrosion potential

As a macrocell is formed the potentials of the components are shifted to less negative values for the anodic components, and to less positive values for the cathodic components (see Fig. 2). From the previously discussed experiment it is clear that passive steel experiences a strong cathodic polarisation when coupled to corroding steel. Experiments were conducted to investigate the influence of macrocells on corrosion potentials E_{corr}, as measured with a reference electrode.

The measurement of the steady-state potentials E_{corr}, present on the surface of corroding reinforced concrete structure has come to be known as half-cell or potential mapping. This technique is now widely accepted as a method of detecting the likelihood of corrosion of steel reinforcement in concrete. The potential mapping technique relies on the presence of differences in electrochemical potential at different points at the steel-concrete interface. The measurement involves the use of a reference electrode which is placed on the concrete surface. The electrode is electrically connected with the underlying reinforcement steel through a high impedance voltmeter.

The surface corrosion potentials of the single corroding and passive steel bars were monitored with an Ag/AgCl-reference electrode (–238 mV vs. SHE) placed on the top and bottom concrete surface, respectively. In the following, corrosion potential values will be given with respect to the Ag/AgCl-reference electrode. Since chloride is added to the mix ingredients, active corrosion of the mild steel bars will ensue immediately during casting, resulting in very negative values for E_{corr}.

The experiments involved macrocells comprising one of the corroding bars and one of the passive bars. Prior to and during coupling the corrosion potentials of the individual bars were measured. Fig. 9 shows the results for the four passive steel bars when coupled to ACT50 (E_{corr} = –467 mV) and ACT75 (E_{corr} = –299 mV), respectively. Due to strong cathodic polarisation the potential of the passive steel bars is shifted towards values close to the corrosion potential of the anodic component. Consequently, according to many codes of practice, passive steel areas will be erroneously identified as actively corroding.

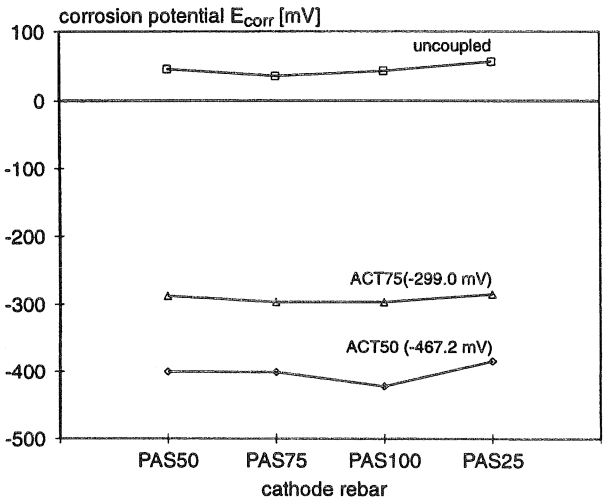

Fig. 9. Development of E_{corr} of passive steel bars prior to and during galvanic coupling to one corroding steel bar.

Influence of macrocells on corrosion rate

The presence of macrocells influences local corrosion rates. In general, the magnitude of the galvanic current underestimates the actual corrosion rate, see Berke et al. (1990) and González et al. (1988). However, using Equations (4) and (5), the initial corrosion rate I_{corr} and the actual corrosion rate I_a can be calculated. For practical purposes, conversion of the results from polarisation measurements to corrosion rates is strictly possible for general corrosion. Chloride-induced corrosion is generally associated with strongly localised attack. Therefore, the averaged corrosion current densities i_{corr} have to be evaluated with some caution although it is likely that for excessive levels of chloride contamination more or less general corrosion may be observed.

The experiments involved sixteen different two-component active/passive macrocells. This was achieved by shortcircuiting one of the actively corroding bars in the top layer (denoted by ACT) with one of the passive stainless steel bars in the bottom layer (denoted by PAS) through an external measuring circuit. The initial potential differences U_{oc} ranged from 320 to 560 mV. Upon shortcircuiting a macrocell developed resulting in steady-state macrocell currents varying from 1.1 μA to 7.0 μA, whereas the average anodic overvoltages achieved were 3.3 mV (ACT75), 6.1 mV (ACT100), 7.2 mV (ACT50) and 33.7 mV (ACT25). Using Eq. (4) I_{corr} can be calculated for each of the corroding bars. The results are shown in Fig. 10. The average values amount to 1.62 μA (ACT25), 2.52 μA (ACT50), 0.85 μA (ACT75) and 0.80 μA (ACT100). Except for rebar ACT25 these results demonstrate a good reproducibility which suggests that the method is applicable for practical situations, see Gulikers (1994).

In Fig. 11, I_{corr} is given as a function of I_{gal} (excluding the results obtained for ACT25). Although there is a general trend that I_{corr} increases as I_{gal} increases, results from galvanic testing have to be interpreted with much caution. For the macrocells investigated, the magnitude of I_{gal} severely

underestimates I_{corr}. It is obvious that measurement of I_{gal} alone gives no reliable information regarding the actual corrosion rates.

Due to anodic polarisation the corrosion rate of the mild steel bars was increased by 58% (ACT25), 20% (ACT50), 17% (ACT75), and 9% (ACT100). The great differences are caused by the different cathodic to anodic surface area ratios. In general, a higher area ratio will result in a greater increase in the corrosion rate. The given sequence follows this common trend.

However, it must be borne in mind that in practice greater area ratios may be present and consequently the corrosion rate may be increased more significantly than presented here.

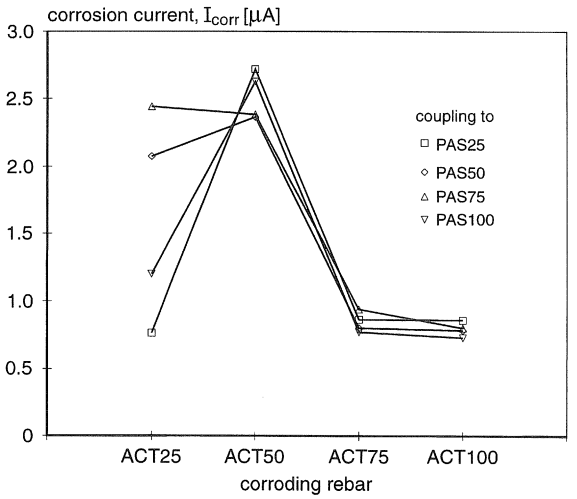

Fig. 10. Corrosion rate I_{corr} of the individual corroding rebars as derived from galvanic testing.

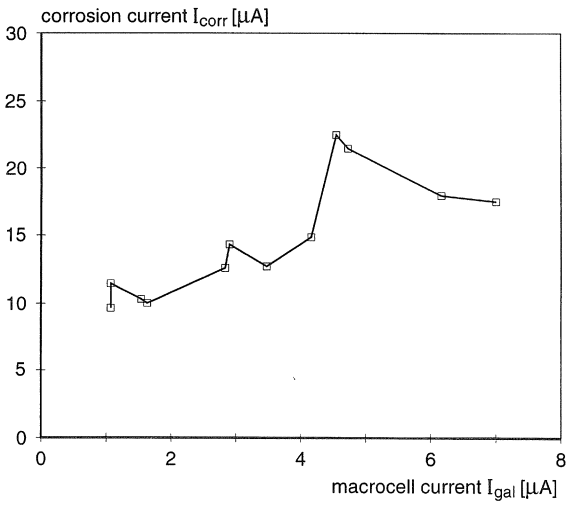

Fig. 11. Corrosion rate I_{corr} as a function of I_{gal} for active/passive macrocells.

Concluding remarks

Under practical conditions of reinforcement corrosion multi-component macrocells consisting of a great number of steel sections exhibiting different electrochemical behaviour will be encountered. Particularly the potential differences developed between actively corroding and passive steel are considered to be of great practical importance since the driving voltage may amount to several hundreds of millivolts, as is verified in this research.

The resistance to cathodic polarisation of the passive stainless steel is strongly dependent on the magnitude of the galvanic current. Generally, the cathodic polarisation resistance dominates and therefore determines the magnitude of the galvanic current to a high degree. However, some caution has to be exercised since the capacity of stainless steel to support cathodic reactions may be different from that of mild steel. Moreover, cathode to anode surface area ratios and geometrical factors have to be taken into account.

Macrocells involving corroding and passive steel reinforcement will result in a very strong change in potential of the passive steel towards more negative values. As a result corrosion potentials may be observed close to that of the anodic component. In these situations potential mapping may erroneously identify passive regions as actively corroding.

For the situations investigated, the electrolytic concrete resistance is of minor importance.

The maximum contribution of R_{con} to the overall cell resistance amounts to just 14% which is attained only for a very high value of U_{cell} (700 mV). This conclusion is also supported by the very negative steady-state potential values for the passive steel bars (cathodic components), which are very close to the values measured for the corroding steel bars (anodic components).

Due to macrocell action the corrosion rate is increased, varying from 9% to 58% for the specific conditions investigated in this research. Based on electrochemical theory of macrocell corrosion the initial corrosion rate can be assessed when the overvoltage and the galvanic current are known. The method described gives reproducible results.

Dependent on the anodic overvoltage achieved the magnitude of the galvanic current underestimates the actual corrosion rate I_a. For overvoltages greater than 50 mV it may be assumed that $I_{gal} = I_a$.

However, it has to be emphasized that practical situations of reinforcement corrosion are much more complex than those investigated here. Generally, they involve a multi-component macrocell in a 3-dimensional environment. The resulting electrochemical interaction between the reinforcement bars can then be calculated only by a numerical approach which takes into account the specific electrochemical behaviour of the bars and the distribution of the concrete resistivity, see Gulikers et al. (1996).

Acknowledgement

Part of this research was sponsored by the Netherlands Technology Foundation (STW).

References

Alonso, C., Andrade, C. and González, J.A. (1988), Relation Between Resistivity and Corrosion Rates of Reinforcements in Carbonated Mortar Made With Several Cement Types, *Cement and Concrete Research*, **5**(18), pp. 687–698.

Andrade, C., Castelo, V., Alonso, C. and González, J.A. (1986), The Determination of the Corrosion rate of Steel Embedded in Concrete by the Polarization Resistance and AC Impedance Methods, in *Corrosion Effect of Stray Currents and the Techniques for Evaluating Corrosion of Rebars in Concrete* (Ed. V. Chaker), ASTM STP906, American Society for Testing and Materials, Philadelphia, pp. 43–63.

Andrade, C., Maribona, I.R., Feliu, S., González, J.A. and Feliu, S. Jr. (1992), The Effect of Macrocells Between Active and Passive Areas of Steel Reinforcements, *Corrosion Science* **33**(2), pp. 237–249.

Berke, N.S., Shen, D.F. and Sundberg, K.M. (1990), Comparison of the Polarisation Resistance Technique to the Macrocell Corrosion Technique, in *Corrosion Rates of Steel in Concrete* (Eds. N.S. Berke, V. Chaker and D. Whiting), ASTM STP1065, American Society for Testing and Materials, Philadelphia, pp. 38–51.

Browne, R.D. Durability of Reinforced Concrete Structures (1991), In *The Corrosion of Steel in Concrete* (short course), Oxford.

González, J.A., Feliu, S., Escudero, M.L., Andrade, C. and Macias, A. (1988), Relative Influence of Galvanic Macrocells and Local Microcells in the Corrosion of Reinforced Concrete Structures, *In Proceedings Measurements and Testing in Civil Engineering*, Lyon, Vol.1, pp. 237–250.

Gulikers, J.J.W. and Van Mier, J.G.M. (1992), Accelerated Corrosion by Patch Repairs of Reinforced Concrete Structures, *In Rehabilitation of Concrete Structures* (Eds. D.W.S. Ho and F. Collins), RILEM, pp. 341–353.

Gulikers, J.J.W. and Van Mier, J.G.M. (1994), Determination of the Corrosion Rate of Steel Reinforcement by Galvanic Testing, *In Corrosion and Corrosion Protection of Steel in Concrete* (Ed. R.N. Swamy), Sheffield Academic Press, pp.2 47–257.

Gulikers, J.J.W. and Schlangen, E. (1996), Numerical Analysis of Galvanic Interaction in Reinforcement Corrosion, *In Corrosion of Reinforcement in Concrete Construction* (Eds. C.L. Page, K.J.W. Treadaway and P.B. Bamforth), Society of Chemical Industry, in press.

Gulikers, J.J.W. (1997a), Laboratory Investigations on Reinforcement Corrosion in Chloride-Contaminated Concrete, In *Fourth CANMET/ACI International Conference on Durability of Concrete* (Ed. V.M. Malhotra), Sydney, Australia, to be published.

Gulikers, J.J.W. (1997b), Aspects of Macrocell Corrosion in Reinforced Concrete Structures, in *Third CANMET/ACI International Conference on Advances in Concrete Technology* (Ed. V.M. Malhotra), Auckland, New Zealand, to be published

Naish, C.C., Harker, A. and Carney, R.F.A. (1990), Concrete Inspection: Interpretation of Potential and Resistivity Measurements, In *Corrosion of Reinforcement in Concrete* (Eds. C.L. Page, K.W.J. Treadaway and P.B. Bamforth), Society of Chemical Industry, pp. 314–332.

Raupach, M. (1992), Zur Chloridinduzierten Makroelementkorrosion von Stahl in Beton, Deutscher Ausschuß für Stahlbeton, Beuth Verlag, Heft 433.

SCHIEßL, P., RAUPACH, M. (1990), Influence of Concrete Composition and Microclimate on the Critical Chloride Content in Concrete, In *Corrosion of Reinforcement in Concrete* (Eds. C.L. Page, K.W.J. Treadaway and P.B. Bamforth), Society of Chemical Industry, pp. 49–58.

Appendix

Concrete: *Mixture proportions:* blast furnace slag cement 300 kg/m^3; w/c = 0.60; natural gravel 1850 kg/m^3.
Particle size distribution: 8–16 mm (24%); 408 mm (20%); 2–4 mm (20%); 1–2 mm(10%); 0.25–0.5 mm (9%); 0.125-0.25 mm (8%);
Curing: 2 days in the mould followed by 12 days at 50% R.H. and 20°C